Stromal growth and epithelial cell proliferation in ventral prostates of liver X receptor knockout mice

Hyun-Jin Kim[a], Leif C. Andersson[b], Didier Bouton[c], Margaret Warner[a], and Jan-Åke Gustafsson[a,1]

[a]Department of Biosciences and Nutrition, Karolinska Institutet, Novum S-14186, Sweden; [b]Department of Pathology, Haartman Institute, University of Helsinki, FIN-00014 Helsinki, Finland; and [c]Faculté de Médecine Necker, Université René Descartes Paris V, 75015 Paris, France

Contributed by Jan-Åke Gustafsson, November 7, 2008 (sent for review September 9, 2008)

With specific liver X receptor α and β (LXRα and LXRβ) antibodies, we found that LXRα is strongly expressed in the luminal and basal cells of prostatic epithelium. The ventral prostates (VP) of LXR$\alpha^{-/-}$ mice are characterized by the presence of smooth-muscle actin-positive stromal overgrowth around the prostatic ducts and by numerous fibrous nodules pushing into the ducts and causing obstruction, so that most of the ducts were extremely dilated. BrdU labeling and Ki67 staining revealed epithelial and stromal proliferation in the fibrous nodules. However, the dense stroma surrounding the ducts was not positive for proliferation markers. There was no detectable difference between WT and LXR$\alpha^{-/-}$ mice VP in the expression of the androgen receptor, but there was an increase in nuclear expression of Snail and Smad 2/3, indicating enhanced TGF-β signaling. Upon treatment of WT mice for 3 months with the LXR agonist T2320 or for 3 weeks with β-sitosterol, LXRα was downregulated, and a VP phenotype similar to that of LXR$\alpha^{-/-}$ mice resulted. We conclude that in rodents, LXRα seems to control VP stromal growth and that LXR$\alpha^{-/-}$ mice may be a useful model to study prostatic stromal hyperplasia. Because LXRα is expressed in the epithelium, the excessive stromal growth in LXR$\alpha^{-/-}$ mice indicates that LXRα is essential for epithelial stromal communication.

Benign prostatic hyperplasia | liver X receptor | TGF-β | mesenchymal transformation | snail

Liver X receptor α and β (LXRα and LXRβ) are members of the nuclear receptor supergene family of ligand-activated transcription factors (1–3). LXRα and -β knockout mice have revealed that LXRα but not LXRβ plays an important role in cholesterol homeostasis, whereas LXRβ has key functions in the immune system, testis, adrenal gland, pancreas, and CNS (4–12). The endogenous ligands of LXR are oxysterols (13, 14), but they also accept phytosterols, particularly β-sitosterol, as ligands (15). Because β-sitosterol is thought to be the active ingredient in the over-the-counter preparation used for relief of the symptoms of benign prostatic hyperplasia (BPH) (16), we investigated the role of LXR in the prostate and the possibility that the beneficial effects of β-sitosterol are mediated by LXR (17).

BPH is a very common disorder in men aged 50 years and is characterized by lower urinary tract disorders that have severe effects on quality of life (18–21). One of the current theories for the mechanism of BPH is that autocrine and paracrine signaling from stromal cells to epithelium creates a focal area of reawakening of epithelial budding and BPH nodule formation (22). The signaling molecules most commonly implicated in the etiology of BPH are TGF-β, FGF, EGF, and insulin-like growth factor (22). Current surgical treatments are associated with risk of urinary incontinence, and current pharmacologic intervention is not always effective. Many men try phytotherapy (use of plants and herbs) for relief of the symptoms of BPH. The most popular phytotherapy is β-sitosterol and saw palmetto (*Serenoa repens*). Saw palmetto has been tested in multiple trials (reviewed in ref. 23). Although in clinical trials saw palmetto has had beneficial effects on urinary flow, no satisfactory explanation for its mechanism of action has been offered. In the present study we investigated whether LXRs play any role in prostatic growth and whether the beneficial effects of β-sitosterol in BPH might be mediated by LXR.

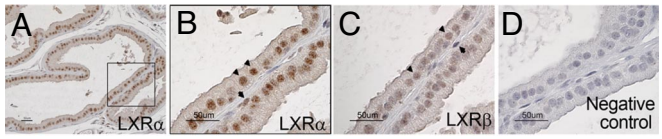

Fig. 1. Localization of LXRα and LXRβ in the mouse VP. LXRα-positive nuclei are localized in epithelial cells (black arrowheads in *B*). Some basal cells (black arrow in *B*) are also positive. LXRβ-positive nuclei (*C*) are localized in a similar pattern as LXRα-positive nuclei in the epithelium (black arrowheads in *C*) and in some basal cells (black arrow in *C*), but the signals are not as strong as with the LXRα antibody. There is no detectable staining in the tissue incubated without primary antibody (negative control, *D*). *B* is a close-up view of the area indicated in *A*. (Scale bars: 50 μm.)

Results

Expression of LXRα and LXRβ in the WT Mouse Ventral Prostate. In the ventral prostate (VP) of WT mice, LXRα was specifically localized in the nuclei of the epithelial cells (Fig. 1 *A* and *B*; black arrowheads in Fig. 1*B*), with some basal cells also positive (black arrow in Fig. 1*B*). The pattern of expression of LXRβ was similar to that of LXRα, but signals were weak (Fig. 1*C*; black arrowheads for epithelial cells, black arrow for basal cell). There was no observable nuclear staining in the tissue incubated without primary antibody (Fig. 1*D*) or with either LXR antibody after preabsorption with their respective LXR proteins (data not shown).

Morphologic Changes in VP of LXR Knockout Mice. The VP of WT control mice appeared histologically normal, with prostatic ducts lined by a single layer of columnar or cuboidal epithelium overlying cells on the basal membrane with little stroma surrounding prostatic ducts (Fig. 2 *A*, *E*, and *I*). In 6-month-old LXR$\alpha^{-/-}$ mice there were several fibrous nodules in the VP ducts (Fig. 2*B*). Many of these nodules were composed of spindle-shaped cells surrounded by a single layer of epithelial cells with pleomorphic nuclei. In some nodules the epithelial layer was lost, and the spindle-shaped cells formed a mass embedded in an extracellular matrix, which could be visualized with toluidine blue staining [Fig. S1].

Author contributions: H.-J.K. performed research; H.-J.K., L.C.A., and M.W. analyzed data; D.B. contributed new reagents/analytic tools; H.-J.K., M.W. and J.-Å.G. designed research; and H.-J.K., M.W., and J.-Å.G. wrote the paper.

Conflict of interest statement: Jan-Åke Gustafsson is shareholder and consultant of KaroBio AB.

[1]To whom correspondence should be addressed. E-mail: jan-ake.gustafsson@ki.se.

This article contains supporting information online at www.pnas.org/cgi/content/full/0811295106/DCSupplemental.

© 2009 by The National Academy of Sciences of the USA

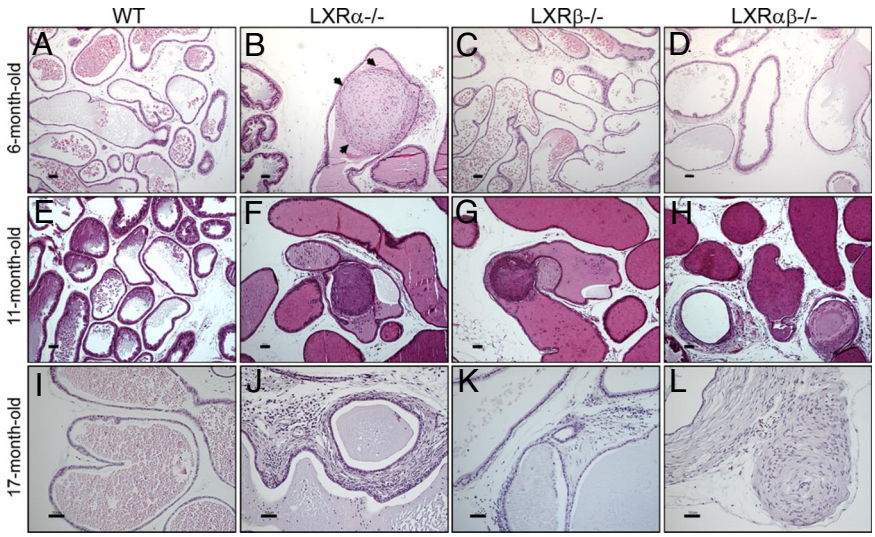

Fig. 2. Representative sections of VP. Morphologic changes of VP of LXR$\alpha^{-/-}$ (*B*, *F*, and *J*), LXR$\beta^{-/-}$ (*C*, *G*, and *K*), LXR$\alpha\beta^{-/-}$ (*D*, *H*, and *L*), and WT (*A*, *E*, and *I*) mice at ages 6 months (*A–D*), 11 months (*E–H*), and 17 months (*I–L*). The ducts in the VP of LXR$\alpha^{-/-}$ mice were filled with several layers of spindle-shaped cells (black arrows in *B*). Slides were stained with H&E (*A–L*). (Scale bars: *A–H*, 100 μm; *I–L*, 50 μm.)

The VP of 6-month-old LXR$\beta^{-/-}$ mice were morphologically indistinguishable from those in age-matched WT mice (Fig. 2*C*), but in 6-month-old LXR$\alpha\beta^{-/-}$ mice there was an increase in intraductal stroma (Fig. 2*D*). The abnormal morphology of the VP in LXR knockout mice increased markedly with age. At age 11 months in LXR$\alpha^{-/-}$ mice (Fig. 2*F*), LXR$\beta^{-/-}$ mice (Fig. 2*G*), and LXR$\alpha\beta^{-/-}$ mice (Fig. 2*H*) there were many more nodules in the lumen of prostatic ducts, with infiltration of mononuclear leukocytes. At age 17 months in LXR$\alpha^{-/-}$ and LXR$\alpha\beta^{-/-}$ mice there was pronounced stromal overgrowth around the prostatic ducts (Fig. 2 *J* and *L*), and in 2-year-old LXR$\alpha^{-/-}$ mice (Fig. 3 *B–D*) there were distended large atrophic prostatic ducts surrounded by multiple layers of dense stroma. At any age there were no lesions detectable in the VP of WT mice (Fig. 2 *A*, *E*, and *I* and Fig. 3*A*).

The multiple layers of stroma around ducts of the VP of LXR$\alpha^{-/-}$ mice contained many smooth-muscle actin-positive cells (Fig. 4*B*). This was also true of some ducts in the LXR$\alpha\beta^{-/-}$ mice (Fig. 4*D*). Very little smooth-muscle actin-positive stroma was found in LXR$\beta^{-/-}$ (Fig. 4*C*) or WT mice (Fig. 4*A*).

Effects of 3 Weeks of β-Sitosterol Treatment on LXR$\beta^{-/-}$ Mouse VP. Treatment of 8-month-old WT mice for 3 weeks with β-sitosterol caused no detectable morphologic changes in the VP (Fig. 5 *A* and *B*). However, in 2 of the 5 LXR$\beta^{-/-}$ mice, fibrous nodules developed in the VP after 3 weeks of β-sitosterol treatment (Fig. 5*D*), and this was accompanied by loss of LXRα protein expression in the nuclei of the prostatic epithelium (Fig. 5*H*, red arrows). Expression of LXRα in vehicle-treated LXR$\beta^{-/-}$ mice is shown for comparison (Fig. 5*G*, black arrows). In WT mice there was clear nuclear staining of LXRα in the epithelial cells of the VP ducts in both untreated and β-sitosterol-treated mice (Fig. 5 *E* and *F*, black arrows).

Effect of Short-Term (3 Weeks) and Long-Term (3 Months) Treatment with LXR Agonist, T2320. In 8-month-old WT mice, 3 weeks of treatment with T2320 caused no significant macroscopic or microscopic changes in the VP (Fig. 6 *A* and *B*) and no detectable change in the expression of LXRα (Fig. 6 *E* and *F*, black arrows). However, after 3 months of T2320 treatment, multiple fibrous nodules were observed in the VP ducts in WT mice (Fig. 6*D*), and there was a clear decrease in LXRα expression in the epithelial cells of the VP (Fig. 6*H*, red arrows).

Measurement of Epithelial Cellular Proliferation by BrdU Incorporation. It is well known that in the adult mouse the proliferation rate in the prostatic epithelium is extremely low. To label the DNA of proliferating cells it was necessary to deliver BrdU every 12 h for 3 consecutive days. Proliferation in columnar epithelial cells located in actively secreting ducts and cuboidal epithelial cells located in inactive ducts were evaluated separately (24). At 6 months of age, in all of the LXR mutant mice, the number of BrdU-positive columnar epithelial cells was higher than in WT mice. The values (mean ± SD) per 1,000 cells were as follows: for WT mice, 21 ± 4; for LXR$\alpha^{-/-}$ mice, 51 ± 34 ($P < 0.05$); for LXR$\beta^{-/-}$ mice, 50 ± 5; and for LXR$\alpha\beta^{-/-}$ mice, 72 ± 17 ($P < 0.001$) (Fig. 7*A*). In ducts with cuboidal cells, there were fewer BrdU-positive cells in WT (6 ± 3) or LXR$\alpha^{-/-}$ mice (10 ± 6), whereas the values were

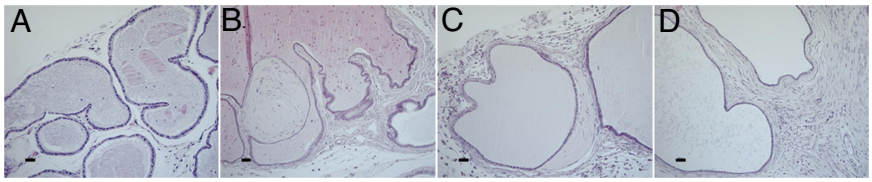

Fig. 3. Severe stromal growth in 2-year-old LXR$\alpha^{-/-}$ mouse VP. At age 2 years, LXR$\alpha^{-/-}$ mouse VP shows multiple stromal layers surrounding distended atrophic prostatic ducts (*B–D*). Some nodules are found in the VP ducts (*B*). As WT mice aged, stroma remained sparse without any nodules (*A*). (Scale bars: 50 μm.)

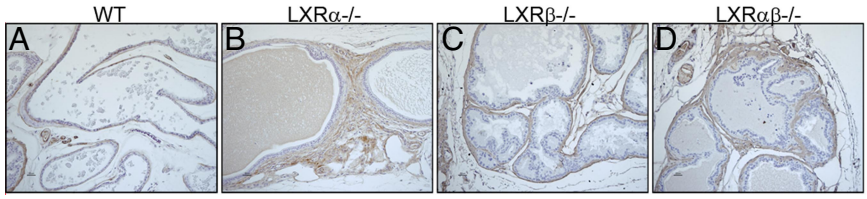

Fig. 4. Smooth-muscle actin immunostaining in the VP of 17-month-old mice. The multiple sheaths of stroma around VP ducts of LXR$\alpha^{-/-}$ mice were immunopositive for smooth-muscle actin (*B*). Some areas of LXR$\alpha\beta^{-/-}$ mouse VP (*D*) had smooth-muscle actin immunopositive stroma, but this was not found in LXR $\beta^{-/-}$ (*C*) or in WT (*A*) mice. (Scale bars: 50 μm.)

31 ± 2 in LXR$\beta^{-/-}$ ($P < 0.001$) and 31 ± 3 in LXR$\alpha\beta^{-/-}$ mice ($P < 0.001$) (Fig. 7*B*).

Increased Epithelial Proliferation (Ki67) in LXR Mutant Mice. At 11 and 17 months of age, few Ki67-positive cells were detectable in VP of WT mice, but in LXR$\alpha^{-/-}$, LXR$\beta^{-/-}$, and LXR$\alpha\beta^{-/-}$ mice, Ki67-positive cells were clearly evident (Fig. 8 *A–D*), particularly in those regions exhibiting ductal hyperplasia in LXR$\alpha^{-/-}$ (Fig. 8*F*), LXR$\beta^{-/-}$ (Fig. 8*G*), and LXR$\alpha\beta^{-/-}$ (Fig. 8*H*) mice. There were few Ki67-positive cells in stroma (Fig. 8*F*).

Increased TGF-β Signaling Through Smad 2/3 and Snail. Smad 2/3 expression was weak in epithelial cells of the VP in WT and LXR$\beta^{-/-}$ mice (Fig. 9 *A* and *C*). However, Smad 2/3 staining was particularly strong in epithelial cells around fibrous bulbs of LXR$\alpha^{-/-}$ (Fig. 9*B*, red arrows) and LXR$\alpha\beta^{-/-}$ mouse VP (Fig. 9*D*, red arrows). A few cells (black arrows in Fig. 9 *B* and *D*) located at the edge of the fibrous bulbs were also weakly positive for Smad 2/3. With specific antibodies raised against Snail, a marker for epithelial mesenchymal transformation (EMT), there was weak staining in the WT and LXR$\beta^{-/-}$ VP epithelial cells (Fig. 9 *E* and *G*) but strong staining in epithelial cells around fibrous bulbs of LXR$\alpha^{-/-}$ (Fig. 9*F*, red arrows) and LXR$\alpha\beta^{-/-}$ mouse VP (Fig. 9*H*, red arrows). The expression of Snail in a few cells surrounding fibrous bulbs was also weakly positive, with a similar pattern as in Smad 2/3 (Fig. 9 *F* and *H*, black arrows).

The expression of Smad 2/3 and Snail was clearly increased in epithelial cells around fibrous nodules in β-sitosterol-treated LXR$\beta^{-/-}$ mice (Fig. 9 *L* and *P*, white arrows) and a few epithelium-like cells surrounding fibrous bulbs in β-sitosterol-treated LXR$\beta^{-/-}$ mice (Fig. 9 *L* and *P*, brown arrows), whereas epithelial cells in VP of vehicle- or β-sitosterol-treated WT mice and vehicle-treated LXR$\beta^{-/-}$ mice occasionally showed very weak staining for Smad 2/3 and Snail (Fig. 9 *I–K* and *M–O*).

Discussion

The physiologic function of LXRs in VP has not hitherto been investigated. In the present study we show that LXRα and LXRβ are expressed in the nuclei of epithelial cells in the VP (Fig. 1). The expression of LXRs in lobes other than the ventral lobe of the prostate was very weak, and these lobes were not studied further.

We observed morphologic changes in the stroma of the VP in LXR$\alpha^{-/-}$, LXR$\beta^{-/-}$, and LXR$\alpha\beta^{-/-}$ mice. The changes became more pronounced as mice aged from 6 months to 11, 17, and 24 months (Figs. 2 and 3). The most conspicuous change in the VP was the formation of fibrous nodules in prostatic ducts. The lesions resembled "Masson bodies" observed in the lungs of patients with bronchiolitis obliterans organizing pneumonia. Little is known about how these nodules are formed (25). In the VP, the areas of mixed stromal and ductal growth showed a pattern similar to growing nodules in BPH samples. At some sites stromal pressure was strong enough to break the epithelial membrane and invade into the lumen of the duct.

In general, overall expression of E-cadherin, one of the key proteins in epithelial cell adhesion, was not changed in LXR$\alpha^{-/-}$, LXR$\beta^{-/-}$, or LXR$\alpha\beta^{-/-}$ mice. However, in the epithelial cells in the local areas where nodules were growing, expression of E-cadherin was reduced or absent (data not shown). Lack of E-cadherin in these areas would be expected to weaken the adhesion between epithelial cells and lead to the observed rupture of the epithelial lining and invasion of stromal cells into the lumen of the duct.

Androgen receptor (AR)-positive cells were specifically localized in the luminal epithelium of the VP in WT mice, and there was no detectable difference in intensity of staining or distribution of AR in LXR$\alpha^{-/-}$, LXR$\beta^{-/-}$, or LXR$\alpha\beta^{-/-}$ mice from that in WT mice (data not shown). In LXR$\alpha^{-/-}$ and LXR$\alpha\beta^{-/-}$ mice, there was increased phospho-Smad 2/3 and

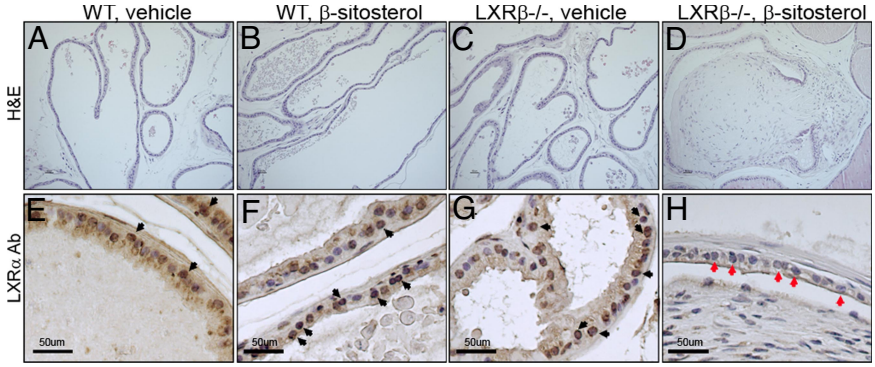

Fig. 5. Effects of 3 weeks β-sitosterol treatment on VP of LXR$\beta^{-/-}$ mice. Treatment of 8-month-old mice for 3 weeks with β-sitosterol led to the formation of nodules in the VP in LXR$\beta^{-/-}$ mice (*D*). Over this period no nodules developed in WT mice (*A*, vehicle; *B*, β-sitosterol) or in vehicle-treated LXR$\beta^{-/-}$ mice (*C*). β-sitosterol-treated LXR$\beta^{-/-}$ mouse VP (red arrows in *H*) showed a decrease of LXRα level compared with vehicle-treated LXR$\beta^{-/-}$ mice (*G*) and WT mice (*E*, vehicle; *F*, β-sitosterol). LXRα-positive cells are indicated by black arrows in *E–G*. (Scale bars: 50 μm.)

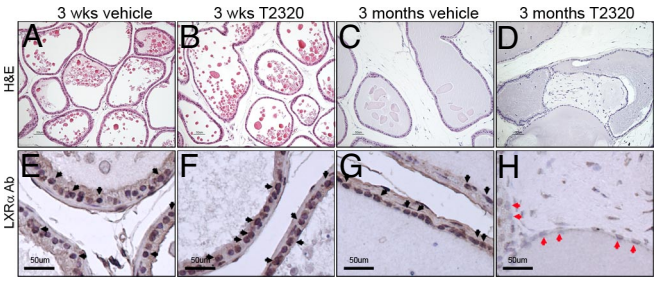

Fig. 6. Long-term (3 months) treatment of T2320 induces the formation of nodules in VP of WT mice. After short-term (3 weeks) exposure to T2320, there were no significant morphologic changes in the VP of WT mice (*A*, vehicle; *B*, T2320). Upon long-term (3 months) treatment with T2320, WT mice developed fibrous nodules in VP ducts (*D*). Over the same period, vehicle-treated WT mice did not develop any nodules (*C*). VP in long-term T2320-treated WT mice (red arrows in *H*) showed a decrease of LXRα level compared with vehicle-treated WT mice (*G*) and short-term-treated WT mice (*E*, vehicle; *F*, T2320). LXRα-positive cells are indicated by black arrows in *E*–*G*. (Scale bars: 50 μm.)

Snail expression in the nuclei of epithelial cells of the VP, in particular in cells surrounding fibrous nodules (Fig. 9). Snail is a strong transcriptional repressor of E-cadherin and is induced by TGF-β signaling. High levels of both Smad 2/3 and Snail proteins indicate enhanced TGF-β signaling.

In BPH, there is increased expression of vimentin in the hyperplastic epithelium (26) and increased TGF-β signaling (27). TGF-β, through activation of the transcription factor SMAD 2/3, plays an important role in EMT. There are very real

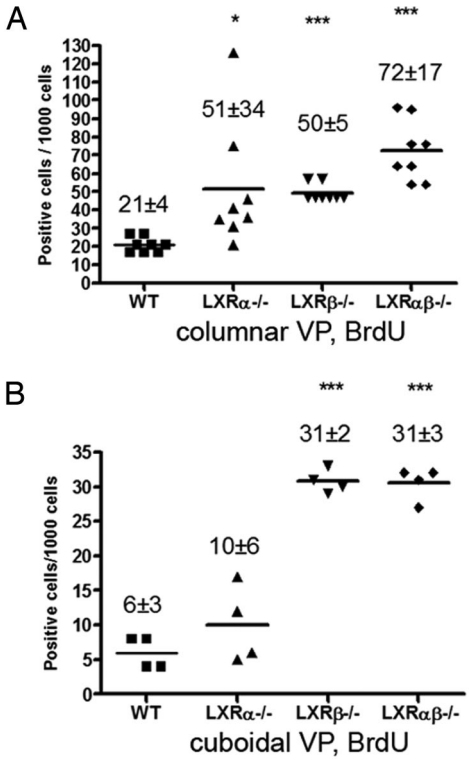

Fig. 7. Increased epithelial proliferation, measured by BrdU incorporation, in VP of 6-month-old LXR mutant mice. Columnar epithelial ducts (*A*) and cuboidal epithelial ducts (*B*) were analyzed separately for BrdU positivity. The results are expressed as positive cells per 1,000 epithelial cells (mean ± SD). At least 4 mice were used for each genotype. *, $P < 0.05$; ***, $P < 0.001$, vs. WT control, Student's *t* test.

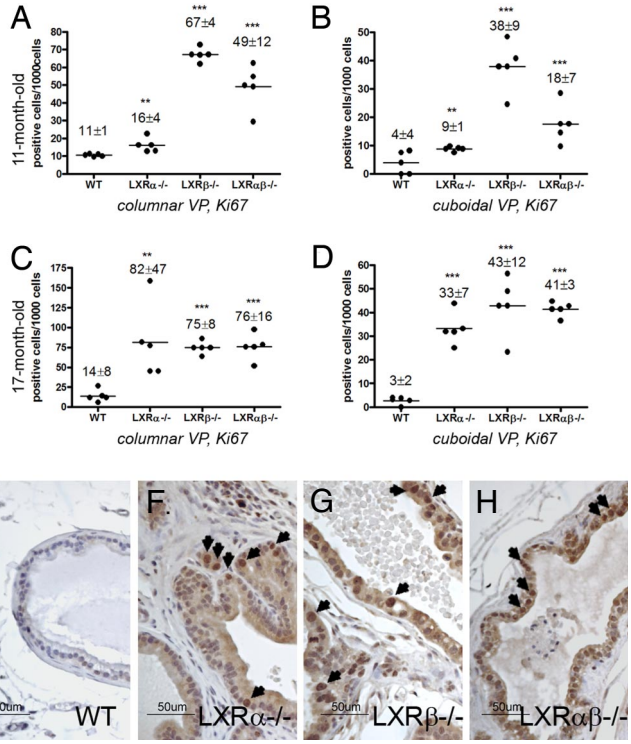

Fig. 8. Increased expression of the proliferation marker, Ki67, in VP of LXR mutant mice at ages 11 months (*A* and *B*) and 17 months (*C*-*H*). Columnar epithelial ducts (*A* and *C*) and cuboidal epithelial ducts (*B* and *D*) were evaluated separately for Ki67-positive epithelial cells. The results are presented as Ki67-positive cells per 1,000 epithelial cells (mean ± SD). Five mice were used for each genotype. **, $P < 0.01$; ***, $P < 0.001$, vs. WT control, Student's *t* test. Representative Ki67 staining in 17-month-old LXR mutant mouse VP compared with WT mice (*E*, WT; *F*, LXR$\alpha^{-/-}$; *G*, LXR $\beta^{-/-}$; *H*, LXR$\alpha\beta^{-/-}$). (Scale bars: *E*–*H*, 50 μm.) Arrows indicate Ki67-positive cell nuclei.

difficulties in studying the etiology of BPH. The first difficulty is the lack of good animal models of the disease. Most rodents and nonhuman primates do not spontaneously develop BPH. Models for BPH are limited to rats and dogs, but they do not mimic all aspects of the human disease (28, 29).

Another difficulty is the morphologic differences between the rodent and human prostate. The human prostate is a single gland with an interior transitional zone next to the urethra, a central zone, and a peripheral zone (30). BPH arises almost entirely in the transitional zone (31). In contrast, there are four distinct prostatic lobes in mouse (anterior, dorsal, lateral, and ventral), which surround the neck of the urinary bladder. It is still not clear which lobe of the rodent prostate most closely resembles the human prostate (28, 32).

In the present study we found a very significant stromal overgrowth accompanied by activation of TGF-β signaling, and increased epithelial proliferation in the prostates of LXR$\alpha^{-/-}$ mice. These data suggest that the origin of the overgrowth of stromal cells around the prostatic ducts is the ductal epithelium. Epithelial cells are the ones that are proliferating and, because there is loss of control of TGF-β signaling, they lose expression of E-cadherin and undergo EMT. This explains why there is no detectable proliferation in the accumulated intraductal stroma.

In addition, β-sitosterol did not cause morphologic changes in the VP of WT mice, but in LXR $\beta^{-/-}$ mice β-sitosterol caused stromal growth similar to what is seen in LXR$\alpha^{-/-}$ mice (Fig. 5). Long-term (3 months) treatment of WT mice with T2320 caused downregulation of the expression of LXRα and

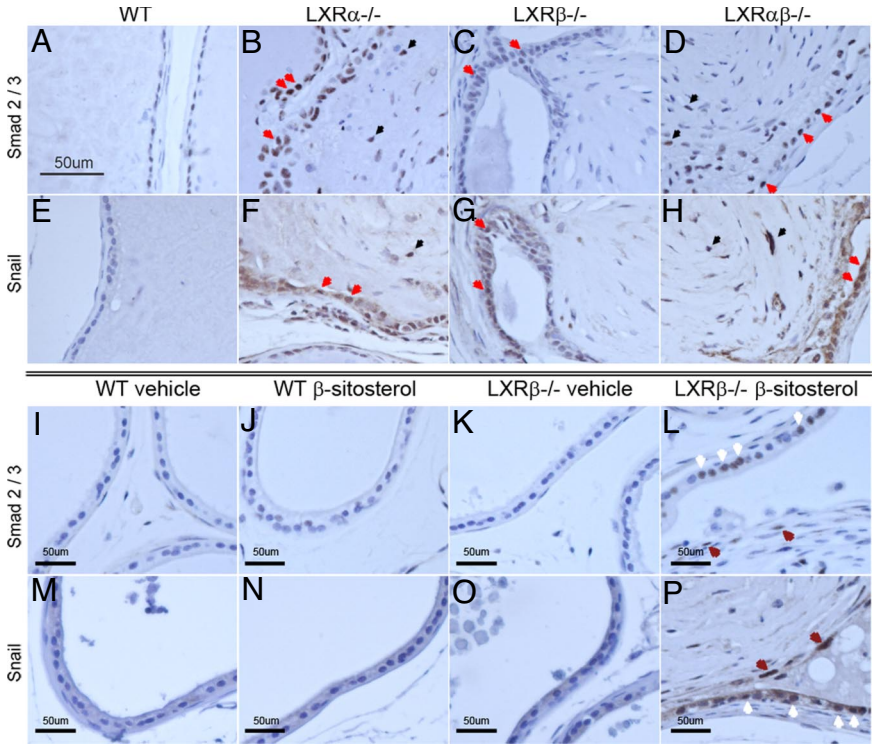

Fig. 9. Increased Smad 2/3 (*A–D*) and Snail (*E–H*) protein in VP epithelial cells around fibrous nodules in LXR mutant mice and in β-sitosterol-treated LXR$\beta^{-/-}$ mice (*L* and *P*). Strong expression of Smad 2/3 and Snail proteins was observed in epithelial cells around the fibrous nodules in LXR$\alpha^{-/-}$ (*B* and *F*) and LXR$\alpha\beta^{-/-}$ (*D* and *H*) mice, whereas in the epithelial cells of WT (*A* and *E*) and LXR $\beta^{-/-}$ (*C* and *G*) mice, staining was very weak or absent. Immune-positive epithelial cells are indicated with red arrows, and immune-positive cells surrounding fibrous bulbs are indicated with black arrows (*B–H*). In β-sitosterol-treated LXR$\beta^{-/-}$mice (*L* and *P*), the expression of Smad and Snail protein was increased, particularly in the epithelial cells (white arrows in *L* and *P*) around the fibrotic nodules and some cells surrounding the fibrous bulbs (brown arrows in *L* and *P*), but not in vehicle-treated WT mice (*I* and *M*), β-sitosterol-treated WT mice (*J* and *N*), or vehicle-treated LXR$\beta^{-/-}$ mice (*K* and *O*) (Scale bars: 50 μm).

stromal overgrowth (Fig. 6). Thus, continuous exposure may not be the optimal regimen for administration of LXR ligands.

In conclusion, our results confirm an important role for LXRs in controlling prostatic growth. LXR$\alpha^{-/-}$ mouse prostates were characterized by several BPH-like features: (*i*) proliferative epithelial cells (Figs. 7 and 8), (*ii*) multiple layers of dense stroma around the prostatic ducts (Figs. 2–4); and (*iii*) dilated prostatic ducts (Fig. 3). Investigation of LXR signaling in the human prostate may shed some light on the etiology of BPH and perhaps lead to development of pharmaceutical drugs targeting LXRs for BPH treatment.

Materials and Methods

Animals. LXR$\alpha^{-/-}$, LXR$\beta^{-/-}$, and LXR$\alpha\beta^{-/-}$ mice were generated by targeted disruption in our laboratory, as previously described (13, 33, 34). All mice were back-crossed for 10 generations. Animals were housed under a 12-h light/12-h dark cycle in the specific pathogen-free facility and were fed a standard mouse chow ad libitum. All experiments were approved by the local Animal Experimentation Ethics Committee for animal experimentation.

Tissue Preparation. Mice were killed by CO_2 asphyxiation. The prostates were removed, and ventral prostate, dorsal prostate, anterior prostate, and lateral prostate were dissected. For immunohistochemical studies, tissues were fixed in 4% paraformaldehyde and embedded in paraffin.

Preparation of Antibodies to LXRα and LXRβ. The goat polyclonal LXRα antibody is directed against the N-terminal region of mouse LXRα, amino acids 68–82. The goat polyclonal LXRβ antibody is directed against the N-terminal region of mouse LXRβ, amino acids 1–17. IgG was purified by polyethylene glycol precipitation and chromatography on Whatman DE52 cellulose. Preabsorbed antibodies were prepared by incubating LXRα or LXRβ antibodies for 12 h at 4 °C with LXRα or LXRβ protein coupled to activated Sepharose (Sigma-Aldrich), respectively (35).

Treatment with BrdU and Analysis. For measurement of proliferation, 4 mice per each group were treated i.p. with BrdU (Roche) at 100 mg/kg every 12 h for 3 days (total of 6 injections).

The paraffin-embedded sections (5 μm) were dewaxed in xylene, rehydrated, processed for antigen retrieval with 10 mM citrate buffer (pH 6.0), and then incubated in 2 M HCl for 10 min at room temperature. This was followed by neutralization in 0.05 M borate buffer (pH 8.5) for 15 min and blocking of endogenous peroxidase with 1% H_2O_2 for 30 min and then in 0.5% Triton X-100 in PBS for 15 min. Sections were then immunostained with anti-BrdU monoclonal antibody overnight at 4 °C, followed by biotinylated goat anti-mouse secondary antibody (1:200) and avidin–biotin peroxidase complex (1:100) for 1 h at room temperature. After sections were washed in PBS, BrdU immunostaining was revealed by using 3,3-diaminobenzidine peroxidase. BrdU-positive columnar epithelial ducts and cuboidal epithelial ducts were separated according to morphologic characteristics, and more than 2,500 epithelial cells were counted separately in each area. The results were recalculated relative to 1,000 epithelial cells and expressed as mean $\pm$ SD.

Administration of β-Sitosterol. Ten WT and 10 LXR$\beta^{-/-}$ male mice (age 8 months) were divided into 4 groups: group 1, WT mice given olive oil only; group 2, WT mice given 42 mg/kg β-sitosterol dissolved in olive oil; group 3, LXR$\beta^{-/-}$ mice given olive oil only; group 4, LXR$\beta^{-/-}$ mice given 42 mg/kg β-sitosterol dissolved in olive oil. Olive oil and β-sitosterol were given daily by gastric gavage for 3 weeks.

LXR Agonist (T2320) Treatment. Eight-month-old WT mice were treated by gastric gavage with T2320 dissolved in olive oil for (*i*) 21 days with 10 mg/kg/day (n = 8) and (*ii*) 3 months with 10 mg/kg/day (n = 8). Control mice (n = 6 for each treatment group) received olive oil only.

Immunohistochemistry. Twenty mice per each group, 6–17 months old, were used. Paraffin sections (5 μm) were dewaxed in xylene, rehydrated, and

processed for antigen retrieval with 10 mM boiling citrate buffer (pH 6.0). The cooled sections were incubated in 1% H_2O_2 for 30 min to quench endogenous peroxidase and then in 0.5% Triton X-100 in PBS for 15 min. Sections were then immunostained with goat anti-LXRα, goat anti-LXRβ, rabbit anti-AR, rabbit anti-E cadherin, rabbit anti-Smad 2/3, rabbit anti-Snail, rabbit anti-Ki67, or mouse anti-smooth-muscle actin in 1% BSA with 0.1% NP_{40} in PBS overnight at 4 °C. 1% BSA replaced primary antibodies in negative controls. After washing, sections were incubated with corresponding secondary antibodies in 1:200 dilutions for 2 h at room temperature. The Vectastain ABC kit (Vector Laboratories) was used for the avidin-biotin complex method according to the manufacturer's instructions. Peroxidase activity was visualized with 3,3-diaminobenzidine (DAKO). The sections were lightly counterstained with hematoxylin, dehydrated through an ethanol series to xylene, and mounted.

ACKNOWLEDGMENTS. This study was supported by grants from the Swedish Research Council, the European Union integrated project CASCADE, and KaroBio AB.

1. Janowski BA, *et al.* (1999) Structural requirements of ligands for the oxysterol liver X receptors LXRalpha and LXRbeta. *Proc Natl Acad Sci USA* 96:266–271.
2. Yang C, *et al.* (2006) Sterol intermediates from cholesterol biosynthetic pathway as liver X receptor ligands. *J Biol Chem* 281:27816–27826.
3. Janowski BA, Willy PJ, Devi TR, Falck JR, Mangelsdorf DJ (1996) An oxysterol signalling pathway mediated by the nuclear receptor LXR alpha. *Nature* 383:728–731.
4. Cha JY, Repa JJ (2007) The liver X receptor (LXR) and hepatic lipogenesis: The carbohydrate-response element-binding protein is a target gene of LXR. *J Biol Chem* 282:743–751.
5. Joseph SB, *et al.* (2002) Direct and indirect mechanisms for regulation of fatty acid synthase gene expression by liver X receptors. *J Biol Chem* 277:11019–11025.
6. Robertson KM, *et al.* (2005) The liver X receptor-{beta} is essential for maintaining cholesterol homeostasis in the testis. *Endocrinology* 146:2519–2530.
7. Steffensen KR, *et al.* (2004) Genome-wide expression profiling: A panel of mouse tissues discloses novel biological functions of liver X receptors in adrenals. *J Mol Endocrinol* 33:609–622.
8. Wang L, *et al.* (2002) Liver X receptors in the central nervous system: From lipid homeostasis to neuronal degeneration. *Proc Natl Acad Sci USA* 99:13878–13883.
9. Andersson S, Gustafsson N, Warner M, Gustafsson JA (2005) Inactivation of liver X receptor beta leads to adult-onset motor neuron degeneration in male mice. *Proc Natl Acad Sci USA* 102:3857–3862.
10. Fan X, Kim HJ, Bouton D, Warner M, Gustafsson JA (2008) Expression of liver X receptor {beta} is essential for formation of superficial cortical layers and migration of later-born neurons. *Proc Natl Acad Sci USA* 105:13445–13450.
11. Gabbi C, *et al.* (2008) Pancreatic exocrine insufficiency in LXRbeta$^{-/-}$ mice is associated with a reduction in aquaporin-1 expression. *Proc Natl Acad Sci USA* 105:15052–15057.
12. Kim HJ, *et al.* (2008) Liver X receptor beta (LXRbeta): A link between beta-sitosterol and amyotrophic lateral sclerosis-Parkinson's dementia. *Proc Natl Acad Sci USA* 105:2094–2099.
13. Alberti S, *et al.* (2001) Hepatic cholesterol metabolism and resistance to dietary cholesterol in LXRbeta-deficient mice. *J Clin Invest* 107:565–573.
14. Alberti S, Steffensen KR, Gustafsson JA (2000) Structural characterisation of the mouse nuclear oxysterol receptor genes LXRalpha and LXRbeta. *Gene* 243:93–103.
15. Chuu CP, Kokontis JM, Hiipakka RA, Liao S (2007) Modulation of liver X receptor signaling as novel therapy for prostate cancer. *J Biomed Sci* 14:543–553.
16. Preuss HG, *et al.* (2001) Randomized trial of a combination of natural products (cernitin, saw palmetto, B-sitosterol, vitamin E) on symptoms of benign prostatic hyperplasia (BPH). *Int Urol Nephrol* 33:217–225.
17. Wilt T, *et al.* (2000) Beta-sitosterols for benign prostatic hyperplasia. *Cochrane Database Syst Rev* CD001043.
18. Avins AL, Bent S (2006) Saw palmetto and lower urinary tract symptoms: What is the latest evidence? *Curr Urol Rep* 7:260–265.
19. Bent S, *et al.* (2006) Saw palmetto for benign prostatic hyperplasia. *N Engl J Med* 354:557–566.
20. Berges RR, Windeler J, Trampisch HJ, Senge T (1995) Randomised, placebo-controlled, double-blind clinical trial of beta-sitosterol in patients with benign prostatic hyperplasia. Beta-sitosterol Study Group. *Lancet* 345:1529–1532.
21. Carraro JC, *et al.* (1996) Comparison of phytotherapy (Permixon) with finasteride in the treatment of benign prostate hyperplasia: A randomized international study of 1,098 patients. *Prostate* 29:231–240, discussion 241–232.
22. Lee KL, Peehl DM (2004) Molecular and cellular pathogenesis of benign prostatic hyperplasia. *J Urol* 172:1784–1791.
23. Wilt T, Ishani A, Mac Donald R (2002) Serenoa repens for benign prostatic hyperplasia. *Cochrane Database Syst Rev* CD001423.
24. Nemeth JA, Lee C (1996) Prostatic ductal system in rats: Regional variation in stromal organization. *Prostate* 28:124–128.
25. Herbut P, Manges E (1945) The ''Masson body'' in rheumatic pneumonia. *Am J Pathol* 21:741–751.
26. Fraga CH, True LD, Kirk D (1998) Enhanced expression of the mesenchymal marker, vimentin, in hyperplastic versus normal human prostatic epithelium. *J Urol* 159:270–274.
27. Zhou W, *et al.* (2003) Dual regulation of proliferation and growth arrest in prostatic stromal cells by transforming growth factor-beta1. *Endocrinology* 144:4280–4284.
28. Lamb DJ, Zhang L (2005) Challenges in prostate cancer research: Animal models for nutritional studies of chemoprevention and disease progression. *J Nutr* 135:3009S–3015S.
29. Marinese D, Patel R, Walden PD (2003) Mechanistic investigation of the adrenergic induction of ventral prostate hyperplasia in mice. *Prostate* 54:230–237.
30. Blacklock NJ (1977) The morphology of the parenchyma of the prostate. *Urol Res* 5:155–156.
31. Kaplan SA, Te AE, Pressler LB, Olsson CA (1995) Transition zone index as a method of assessing benign prostatic hyperplasia: Correlation with symptoms, urine flow and detrusor pressure. *J Urol* 154:1764–1769.
32. Abate-Shen C, Shen MM (2002) Mouse models of prostate carcinogenesis. *Trends Genet* 18:S1–S5.
33. Schuster GU, *et al.* (2002) Accumulation of foam cells in liver X receptor-deficient mice. *Circulation* 106:1147–1153.
34. Steffensen KR, Robertson K, Gustafsson JA, Andersen CY (2006) Reduced fertility and inability of oocytes to resume meiosis in mice deficient of the Lxr genes. *Mol Cell Endocrinol* 256:9–16.
35. Toresson G, *et al.* (2004) Purification of functional full-length liver X receptor beta produced in *Escherichia coli*. *Protein Expr Purif* 35:190–198.